

Nucleosynthesis in Outflows from the Inner Regions of Collapsars

Jason Puet¹, Todd A. Thompson^{2,3} & R. D. Hoffman¹

ABSTRACT

We consider nucleosynthesis in outflows originating from the inner regions of viscous accretion disks formed after the collapse of a rotating massive star. We show that wind-like outflows driven by viscous and neutrino heating can efficiently synthesize Fe-group elements moving at near-relativistic velocities. The mass of ^{56}Ni synthesized and the asymptotic velocities attained in our calculations are in accord with those inferred from observations of SN1998bw and SN2003dh. These steady wind-like outflows are generally proton rich, characterized by only modest entropies, and consequently synthesize essentially nothing heavier than the Fe-group elements. We also discuss bubble-like outflows resulting from rapid energy deposition in localized regions near or in the accretion disk. These intermittent ejecta emerge with low electron fraction and are a promising site for the synthesis of the $A = 130$ r -process peak elements.

Subject headings: gamma rays: bursts—nucleosynthesis—accretion disks

1. Introduction

In this paper we examine the production of nuclei in matter escaping the innermost regions of collapsars. Collapsars occur when the usual neutrino-powered supernova shock fails to expel the mantle of a rotating massive star whose core has collapsed (Woosley 1993; MacFadyen & Woosley 1999). The inner parts of the star collapse to form a disk accreting rapidly onto a central black hole. Interesting elements, and in particular ^{56}Ni and $A = 130$ peak r -process elements, may be synthesized in outflows from the inner regions of this disk.

¹N-Division, Lawrence Livermore National Laboratory, Livermore CA 94550;
 pruet1@llnl.gov,rdhoffman@llnl.gov

²Hubble Fellow

³Astronomy Department and Theoretical Astrophysics Center, 601 Campbell Hall, The University of California, Berkeley, CA 94720; thomp@astro.berkeley.edu

Understanding how collapsars make ^{56}Ni , whose decay fuels optical light curves of SNe, is central to connecting the deaths of massive stars with Gamma Ray Bursts (GRBs). There are now observations of SN-like light curves for some five or six GRBs (Price et al. 2003). For two SNe/GRBs (SN 1998bw–Galama (1998) and SN2003dh–Stanek et al. (2003); Hjorth et al. (2003)) there are detailed estimates of Ni ejecta mass and velocity (Patat et al. (2001); Iwamoto et al. (1998); Woosley, Eastman, & Schmidt (1999) for SN1998bw and Hjorth et al. (2003); Woosley & Heger (2003) for SN2003dh).

Though it is generally agreed that collapsars are promising sources for the observed Ni, details remain uncertain. There are several possibilities. As in “ordinary” SNe, Ni may be synthesized explosively as a strong shock traverses the stellar mantle. Parametrized piston-driven simulations of the explosion of massive stars (Woosley & Heger 2003) and simulations of massive stars exploded by outgoing bi-polar jets (Maeda & Nomoto 2003) show that this mechanism may produce substantial amounts of fast moving Ni. It is not clear, though, if explosive burning can account for the very fast ($v \gtrsim 0.1c$) and massive ($M_{\text{Ni}} \approx 0.5M_{\odot}$) outflows seen in SN2003dh. Another possibility is that the Ni is synthesized in some sort of slow, heavily baryon polluted outflow formed above the black hole (Nagataki et. al 2003). The last possibility, investigated here, is that Ni is synthesized in wind-like outflows from the accretion disk (MacFadyen & Woosley 1999; MacFadyen 2003). Those authors find, for plausible disk viscosities and accretion rates, fast ($v \sim 4 \times 10^9 \text{ cm s}^{-1}$) Ni-rich outflows blown off of the inner accretion disk by viscous heating. We provide a simple treatment of these winds with an eye toward understanding the wind energetics and the conditions needed for efficient Ni synthesis.

We also discuss the possibility of synthesizing *r*-process elements in collapsar events. The *r*-process (Burbidge et al. 1957; Cameron 1957) accounts for roughly half the heavy nuclides above the iron group, producing characteristic abundance peaks at $A \sim 80, 130$, and 195 . The astrophysical site for the production of these elements remains uncertain. By examining the relative isotopic abundances of $^{182}\text{Hf}/^{180}\text{Hf}$ and $^{129}\text{I}/^{127}\text{I}$, Wasserburg, Busso, & Gallino (1996) argued that at least two distinct *r*-process sites, operating in the galaxy with different rates, must produce the nuclides with $A \lesssim 130$ and $A \gtrsim 130$ (see also Wasserburg & Qian 2000). Subsequent work by Qian, Vogel, & Wasserburg (1998) and Qian & Wasserburg (2000) argues that events which produce the heavy, third-peak nuclei occur ten times more frequently than events which produce the lighter (second peak and below) elements. The latter must also produce iron-group elements copiously. Conversely, the high frequency (producing $A \sim 195$) must produce little iron. The association of lower event frequency with large Ni production, plus the work of Heger et al. (2003), which argues that the collapsar rate might be $\sim 10\%$ of the total core-collapse supernova rate, points potentially to collapsar events as the astrophysical site for $A \lesssim 130$ *r*-process element synthesis. We argue that the

inner collapsar disk material with low electron fraction may be ejected rapidly, with modest entropy, in magnetically dominated filaments or bubbles and that this intermittent outflow is a likely site for r -process nucleosynthesis up to $A \sim 130$.

2. Disk Outflows and Nucleosynthesis

Nucleosynthesis in outflows from the disk is primarily sensitive to the electron fraction (Y_e), the entropy per baryon (s/k_b), and the timescale characterizing the expansion of the fluid around the time of efficient α -particle formation (Hoffman, Woosley, & Qian 1997). To estimate these quantities we examine two different, and in some sense limiting, realizations of the outflow. The first is a hydrodynamic picture of the outflow, which assumes the presence of stable and ordered pressure profiles: a steady disk wind. The second picture we examine is one where rapid magnetic reconnection or turbulent viscous heating deposits entropy (and energy) in localized “bubbles” within the disk, causing rapid ejection of low Y_e material. Both types of processes likely occur to some extent.

3. A Hydrodynamic Wind Picture

Steady or quasi-steady spherical winds have been extensively used to study nucleosynthesis in the neutrino-driven wind occurring several seconds after core bounce in core-collapse SNe (Duncan, Shapiro, & Wasserman 1986; Woosley et al. 1994; Takahashi, Witt, & Janka 1994; Qian & Woosley 1996; Cardall & Fuller 1997; Sumiyoshi et al. 2000; Otsuki et al. 2000; Wanajo et al. 2001; Thompson, Burrows, & Meyer 2001). Of particular interest to the present study is the paper by Qian & Woosley (1996), which provided insight into and analytic expressions for describing the connection between the various parameters determining the wind itself (neutron star radius and mass, neutrino luminosities, etc.) and the properties of the flow that determine the resulting nucleosynthesis: the electron fraction, entropy, and dynamical timescale. It should be noted that so far no agreed upon neutron star wind solutions give a robust r -process (with the possible exception of winds from very relativistic neutron stars (Cardall & Fuller 1997; Thompson, Burrows, & Meyer 2001) or highly magnetic neutron stars (Thompson 2003)).

In this section we describe our simple model of time-independent disk winds, akin to the models previously developed in the neutron star context. Roughly, our assumption of a steady-state outflow is an attempt to use an estimate of the vertical disk pressure gradient to derive the dynamical timescale of the outflow and the increase in entropy due to viscous and

neutrino energy deposition. Because we parameterize flow streamlines and currently employ only a local α -disk prescription for energy deposition, our analysis is limited and must be tested eventually against full MHD simulations of collapsar disk winds.

3.1. Equations

The equations governing the wind structure are determined by mass, momentum, energy, and lepton number conservation. For steady flow these are, respectively,

$$\nabla \cdot (\rho u) = 0 \quad (1)$$

$$\rho u \cdot \nabla u = \vec{f} \quad (2)$$

$$u \cdot (\nabla \cdot T) = -u \cdot (\nabla \cdot T_\alpha) + q_\nu \rho N_a \quad (3)$$

$$u \cdot (\nabla Y_e) = -\lambda_{e^-p} \left(Y_e - \frac{1 - X_{\text{free}}}{2} \right) + \lambda_{e^+n} \left(1 - Y_e - \frac{1 - X_{\text{free}}}{2} \right). \quad (4)$$

Here ρ is the mass density, u is the velocity, q_ν is the net neutrino energy deposition rate per baryon, and \vec{f} is the force (gravitational+viscous+pressure gradient) acting on outflowing fluid elements. $T = \rho u \otimes u + pg$ is the stress-energy tensor of the fluid, with p the pressure and g the metric tensor. Our treatment is entirely Newtonian, and in spherical polar coordinates ($1 = r$, $2 = \theta$, $3 = \phi$) $g_{11} = 1$, $g_{22} = r^2$, $g_{33} = r^2 \sin^2 \theta$, and $g_{ij} = 0$ for $i \neq j$. Including relativistic effects in aspherical viscous flows is straightforward, but more complicated than including relativistic effects for inviscid spherical outflows from neutron stars.

In eq. (4) we have approximated the flow as consisting of free nucleons and α -particles, Y_e is the net number of protons per baryon in the flow, λ_{e^-p} and λ_{e^+n} are the rates for electron and positron capture on free nucleons (e.g. Qian & Woosley 1996), and X_{free} is the mass fraction of free nucleons in the flow. Lepton capture on heavy nuclei is typically very slow compared to lepton capture on free nucleons and is neglected here. When $X_{\text{free}} = 0$ (all α -particles), then, eq. (4) gives zero rate of change for Y_e . We approximate X_{free} as

$$X_{\text{free}} = 8.2 \cdot 10^8 \frac{T_{\text{MeV}}^{9/8}}{\rho^{3/4}} \exp \left(\frac{-7.074}{T_{\text{MeV}}} \right) \quad (5)$$

or unity, whichever is smaller (Woosley & Baron 1992). Here T_{MeV} is the temperature in MeV. Eq. (4) does not account for the influence of neutrino capture on Y_e . Including neutrinos in a reliable way is beyond the scope of this paper. However, in section 3.2.2 we outline in general terms how neutrinos are expected to influence Y_e .

The viscous stress tensor is (e.g. Mihalas & Mihalas (1984))

$$T_\alpha = 2\mu D, \quad (6)$$

with

$$D^{xy} = \frac{1}{2} (u_x^y + u_y^x). \quad (7)$$

Here a semi-colon represents the covariant derivative. Following Stone, Pringle & Begelman (1999), we neglect all components of D except $D^{r\phi} = D^{\phi r} = (1/2)u_{,r}^\phi$ and $D^{\theta\phi} = D^{\phi\theta} = (1/2r^2)u_{,\theta}^\phi$. The neglect of the other components of the stress tensor is justified if the magnetic instabilities providing the shear stresses produce small poloidal stresses. For the coefficient of shear viscosity we adopt the parametrization often used in studies of viscous disks: $\mu = \alpha p/\Omega_k(r_0)$. Here α is the standard disk alpha parameter (Shakura & Sunyaev 1973), r_0 is the radius from which the wind leaves the disk, and the Keplerian frequency is $\Omega_k(r_0) = \sqrt{GM/r_0^3}$, with M the mass of the central black hole.

To proceed, we parametrize the trajectories of the outflow by $\vec{r} = (r, \theta, \phi) = (r_0 g(\tilde{\theta}), \tilde{\theta}, \phi)$ and the wind velocity by $\vec{u} = (\dot{r}, \dot{\theta}, \dot{\phi}) = (r_0 g' f, f, \xi) \Omega_k(r_0)$. Throughout the paper a prime denotes differentiation with respect to $\tilde{\theta}$. We also define the velocity in the $r - \theta$ plane, $v = f \Omega_k(r_0) \sqrt{g^2 + g'^2}$. The basic idea of parametrizing the trajectories in the way we have comes from the pioneering work of Blandford & Payne (1982). Unlike that work, however, we are not solving for the outflow and magnetic field configuration in a global and self consistent way. Rather, we will choose trajectories $g(\tilde{\theta})$ in order to get estimates of the wind parameters important in determining nucleosynthesis. Solving for the trajectories in a consistent way likely requires a hydromagnetic simulation which can capture the interplay between the outflow and the magnetic field configuration.

With the above definition for the streamlines, eq. (1) becomes

$$\rho v a = \text{Constant}. \quad (8)$$

Here $a = g^3 \sin \theta (g^2 + g'^2)^{-1/2}$ and is proportional to the area defined by fluid streamlines. The equation governing v is found by taking the projection of eq. (2) along the streamlines:

$$vv' \left(1 - \frac{P_{,\rho}}{v^2} \right) = A_v - \frac{P_{,s} s'}{\rho} + P_{,\rho} \frac{a'}{a}, \quad (9)$$

where $P_{,\rho} = \partial P / \partial \rho|_s = c_s^2$, $P_{,s} = \partial P / \partial s|_\rho$, and

$$A_v = r_0^2 \Omega_k^2 \xi^2 \left(\frac{1}{2} g^2 \sin^2 \theta \right)' + r_0^2 \Omega_k^2 \left(\frac{1}{g} \right)' \quad (10)$$

is the sum of the gravitational and centrifugal forces. Eq. (3) can be recast as the equation governing the entropy of the outflow

$$f \Omega_k s' = \frac{\alpha P \sin^2 \theta \Omega_k(r_0)}{\rho T N_a} \left(\left(\frac{3\xi}{2} \right)^2 + \left(\xi' + \frac{3g'\xi}{2g} \right)^2 \right) + \frac{q_\nu}{T}. \quad (11)$$

Here s is the entropy per baryon scaled by k_b . We approximate s as the sum of contributions from relativistic light particles (photons and e^\pm pairs), free nucleons, and alpha particles:

$$s = 5.21 \frac{T_{\text{MeV}}^3}{\rho_8} + X_{\text{free}} \left(12 + \ln \left(\frac{T_{\text{MeV}}^{3/2}}{\rho_8} \right) \right) + \frac{1 - X_{\text{free}}}{4} \left(15.4 + \ln \left(\frac{T_{\text{MeV}}^{3/2}}{\rho_8} \right) \right), \quad (12)$$

where $\rho_8 = \rho/10^8 \text{ g cm}^{-3}$. The influence of nuclear recombination on the wind dynamics is discussed in section 3.2.4. The equation describing the evolution of Y_e is

$$f\Omega_k Y'_e = -\lambda_{e^-p} \left(Y_e - \frac{1 - X_{\text{free}}}{2} \right) + \lambda_{e^+n} \left(1 - Y_e - \frac{1 - X_{\text{free}}}{2} \right). \quad (13)$$

We adopt a crude parametrization for q_ν :

$$q_\nu = q_h - q_c. \quad (14)$$

Neutrino energy loss from the wind occurs principally via e^\pm capture on free nucleons ($e^-p \rightarrow n\nu_e$ and $e^+n \rightarrow p\bar{\nu}_e$). The energy loss rate associated with these processes is $q_c \approx 2.3T_{\text{MeV}}^6$ (MeV/sec baryon). As in the neutrino-driven winds that occur in the late-time core-collapse SN cooling epoch, neutrino heating occurs principally via charged-current neutrino capture on free nucleons ($\nu_e n \rightarrow pe^-$ and $\bar{\nu}_e p \rightarrow ne^+$). The heating rate for these processes is $q_h \approx 5L_{\nu,51}(\langle E_\nu \rangle / 10 \text{ MeV})^2(1/r_7^2)$ (MeV/sec baryon) (Qian & Woosley 1996). Here we have approximated the inner, neutrino luminous portions of the disk as being spherical, $L_{\nu,51}$ is the sum of the ν_e and $\bar{\nu}_e$ neutrino luminosities in units of 10^{51} erg/sec , ϵ_ν is the average ν_e or $\bar{\nu}_e$ energy, and $r_7 = r/10^7 \text{ cm}$.

To get an idea of the relative importance of viscous and neutrino heating, note that for a $3M_\odot$ black hole with Kerr parameter $a = 0$ accreting at $0.1M_\odot \text{ sec}^{-1}$, Popham, Woosley, & Fryer (1999) estimate $L_{\nu,51} \approx 3 - 7$, for α in the range $0.03 - 0.1$. Typical average neutrino energies for these disks are $\langle E_\nu \rangle \approx 15 - 20 \text{ MeV}$. At $r = 10^7 \text{ cm}$, the viscous heating rate is $\approx 140T_{\text{MeV}}(\alpha/0.1)(\text{MeV/sec nucleus})$ for $\xi \approx 1$, while $q_h \approx 100(L_{\nu,51}/5)(\epsilon_\nu/20 \text{ MeV})^2(\text{MeV/sec nucleon})$. For these disks, then, neutrino and viscous heating can be comparable. For a disk surrounding a black hole with high Kerr parameter, neutrino heating can dominate over viscous heating. Popham, Woosley, & Fryer (1999) estimate that a disk with $a = 0.95$ has a neutrino luminosity about eight times larger than the same disk with $a = 0$. As we discuss though, the parameters important for nucleosynthesis are not very dependent on the neutrino luminosity (though the influence of neutrino losses is important in determining the disk structure).

3.2. Wind Profiles: Y_e , s , and τ_{dyn}

With the above formalism we can discuss conditions in outflows from the disk and implications for nucleosynthesis. For simplicity, fluid streamlines are taken to be straight lines making an angle θ_0 with the plane of the disk (or $\pi - \theta_0$ with the z-axis). We assume that ξ decreases with distance z above the disk as

$$\xi = \exp(-z/\xi_z) \quad (15)$$

with ξ_z the scale height for the decrease in ξ . Thus, as the wind moves out of the plane of the disk, its velocity in the ϕ direction evolves as $\xi(z)\Omega_k$. Our discussion and parametrization of these steady state winds is similar in some ways to the work of Daigne & Mochkovitch (2002), who examined the conditions needed for ultra-relativistic (Lorentz factor much larger than unity) outflows from accretion disks.

We do not present an exhaustive survey of wind models – the simplicity of our model probably does not warrant it. Instead we outline how the parameters influencing nucleosynthesis in the wind depend on the character of the accretion disk and on the starting radius of the outflow. In Table 1 we show results from wind solutions for outflows from a moderate viscosity ($\alpha = 0.1$) disk and from a low viscosity ($\alpha = 0.03$) disk. In both cases the accretion rate of the disk is $\dot{M} = 0.1M_{\odot} \text{ sec}^{-1}$. For each type of disk, outflows from a moderate radius ($r_0 = 10^7$) and a small radius ($r_0 = 10^{6.5} \text{ cm}$) are considered. Initial (in-disk) values of the temperature and density for the calculations were taken from the results presented in Popham, Woosley, & Fryer (1999). Typical disk temperatures are a few MeV, typical densities are $\rho \gtrsim 10^9 \text{ g cm}^{-3}$, and typical entropies are of order 5-10. The starting electron fraction was taken from Puet, Woosley, & Hoffman (2003). The electron fraction in the disk depends sensitively on the mass accretion rate and viscosity, and can be anywhere in the range $0.1 \lesssim Y_e \lesssim 0.53$. Results shown in Table 1 were calculated with a neutrino heating rate $q_h = (100/r_7^2)(\text{MeV/sec nucleus})$. We find that changing q_h by a factor of two in either direction does not have a big influence on the asymptotic wind parameters. Increasing q_h by a factor of eight results in an increase in the mass outflow rate of $\approx 25\%$ and in increase in the asymptotic entropy of ≈ 3 units for models C and D. All calculations in Table 1 are for $\theta_0 = 80^\circ$. Effects of changing θ_0 are discussed in §3.3.

To give a point of reference for the following discussion we show typical wind solutions in Figures 1 and 2. Figure 1 corresponds to a wind beginning at $r_0 = 10^7 \text{ cm}$ in a disk with $\alpha = 0.1$ accreting at a rate of $0.1M_{\odot} \text{ sec}^{-1}$ onto a central black hole of mass $3M_{\odot}$. These parameters are close to those thought to describe conditions in collapsars. For the calculation in Fig. 1, $\theta_0 = 80^\circ$ and $\xi_z = 2r_0 = 2 \times 10^7 \text{ cm}$. Figure 2 shows a wind for the same parameters as in Fig. 1 except with $r_0 = \xi_z/2 = 10^{6.5} \text{ cm}$. These winds bear qualitative

similarities to ν -driven winds from neutron stars. The temperature at the base of the wind is approximately that for which the heating and cooling rates balance each other. Also, most of the heating occurs at the base of the flow, with the evolution at larger radii being isentropic.

3.2.1. The Asymptotic Entropy

The trend of greater increase in final entropy with increasing initial gravitational potential and the weak dependence of the final entropy on the heating rate (α) is evident. This is similar to the case for winds from NS's. Qian & Woosley (1996) argued that the final entropy should scale as $\sim r_0^{-2/3}$, with only a weak dependence on the heating rate, which is a fair approximation to the results shown in Table 1. Overall, the final entropies expected for winds from the disk are rather modest ($\sim 30 - 50$) and more typical of the α -process than the r -process.

So far it is not clear to what extent the wind properties relevant for nucleosynthesis are determined by our simplified model and to what extent the wind properties are determined by more basic considerations. To get insight into the distinction note that the hydrodynamic equations can be recast in the form

$$Q' \equiv Ts' = b' \quad (16)$$

with Q the total energy per baryon added to the flow by viscous and neutrino heating and b the Bernoulli integral for this system:

$$b \equiv \frac{m_N v^2}{2} + Ts_{rad} + \frac{5T}{2\bar{A}} + \epsilon_{nuc} - \frac{GMm_N}{r}(1 + U_c) \quad (17)$$

$$\approx 500 \left(\frac{v}{c}\right)^2 + T_{\text{MeV}} s_{\text{rad}} + \frac{5T_{\text{MeV}}}{2\bar{A}} + \epsilon_{nuc} - 45(1 + U_c) \left(\frac{M}{3M_{\odot}}\right) \frac{10^7 \text{cm}}{r} (\text{MeV}). \quad (18)$$

Here s_{rad} is the entropy per baryon in radiation, \bar{A} is the mean atomic mass of bound nuclei and ϵ_{nuc} is the mean nucleon binding energy. If everything burns to α -particles the difference in ϵ_{nuc} before and after nuclear recombination is about 7.074 MeV, while if everything burns to Fe-group nuclei the difference is about 1.4 MeV larger. The quantity U_c accounts for the influence of the ϕ component of the velocity in overcoming the gravitational potential. For example, within the disk $r_0 \dot{\phi} \approx r_0 \Omega_k(r_0)$, so the material already has half the kinetic energy needed to escape the gravitational pull of the black hole. In our treatment

$$U_c = (g/2) \int_{\pi/2}^{\theta} \xi^2 (g^2 \sin^2 \theta)' d\theta. \quad (19)$$

The change in entropy of the outflowing fluid is

$$\Delta s \equiv s_f - s_i = \int_i^f \frac{db}{T}, \quad (20)$$

where the subscripts i and f denote values at the base and end (i.e. asymptote) of the flow respectively. If the temperature decreases along outflowing streamlines

$$\Delta s \gtrsim \Delta b/T_i. \quad (21)$$

Approximate equality in eq. (21) holds if most of the heating occurs very near the base of the flow.

For a given starting radius and disk composition the above considerations give a minimum value for the final entropy as a function of the asymptotic velocity of the outflow and U_c . Values for the different cases considered in the wind calculations are shown in Table 3. The calculations there assume $U_c = 0$ (or equivalently that ξ_z is small). In this case the centrifugal potential plays no role. There is fairly close agreement between the asymptotic entropies found from consideration of the Bernoulli integral and the asymptotic entropies found in our wind calculations (Table 1). Entropies found in our calculations are typically about 5 units lower than the values in Table 3. This arises mostly because our wind calculations have modest ξ_z and the rotational velocity plays some role in decreasing the effective gravitational potential.

3.2.2. The Asymptotic Electron Fraction

In contrast to the way in which the final entropy is set, the final electron fraction in these disk winds is set by quite different factors than in NS winds. In winds from NS's, neutrinos dominate both the energy deposition rates and the lepton capture rates. The neutron to proton ratio comes into approximate equilibrium with the neutrino spectra. Because the neutrinos originate from the neutron rich crust of the neutron star, which has a high opacity to electron neutrinos, the $\bar{\nu}_e$ spectrum is hotter than the ν_e spectrum. Consequently, neutrino capture above the nascent neutron star leads to a neutron-rich wind favorable for the r -process.

In winds from accretion disks that are optically thin to neutrinos all factors conspire to make $Y_e > 0.5$. In the first place, e^\pm capture, rather than neutrino capture, generally sets Y_e in the disk and in the wind. As viscous heating adds entropy to the outgoing fluid the electron degeneracy is removed. Weak equilibrium then favors $Y_e > 0.5$ because of the neutron-proton mass difference.

Secondly, when neutrino captures are important they tend to increase Y_e (Surman & McLaughlin 2003; Beloborodov 2003). Very roughly, this can be thought of as a consequence of the neutrinos carrying net lepton number away from the deleptonizing disk. To make these arguments more quantitative, note that the ratio of the rates for ν_e and $\bar{\nu}_e$ capture is

$$R \equiv \frac{\lambda(\bar{\nu}_e p \rightarrow e^+ n)}{\lambda(\nu_e n \rightarrow e^- p)} = \frac{n_{\bar{\nu}_e}}{n_{\nu_e}} \left(\frac{1.2\langle E_{\bar{\nu}_e} \rangle^2 + \Delta^2 - 2\Delta\langle E_{\bar{\nu}_e} \rangle}{1.2\langle E_{\nu_e} \rangle^2 + \Delta^2 + 2\Delta\langle E_{\nu_e} \rangle} \right) \quad (22)$$

(Qian & Woosley 1996). In eq. (22) $\Delta = 1.293\text{MeV}$ is the neutron-proton mass difference, $\langle E_\nu \rangle$ is the average neutrino energy, and n_ν is the neutrino number density. The factor 1.2 weighting $\langle E_\nu \rangle^2$ is approximate and depends on details of the neutrino spectrum. Taking typical neutrino emission as originating from $r \approx 10^{6.5}\text{cm}$ in the disk, the disk parameters from (Popham, Woosley, & Fryer 1999) and the electron fraction from (Pruet, Woosley, & Hoffman 2003), the ratio in eq. (22) can be calculated (Fuller, Fowler, & Newman 1982). We find $R = 0.94$ for the $\dot{M} = 0.1M_\odot \text{sec}^{-1}$, $\alpha = 0.1$ disk and $R = 0.66$ for the $\dot{M} = 0.1M_\odot \text{sec}^{-1}$, $\alpha = 0.03$ disk. Because $R < 1$, neutrino capture above the disk tends to drive the outflow proton rich.

It is worth noting that in the very inner regions of the disk the composition can fall out of weak equilibrium (Pruet, Woosley, & Hoffman 2003), with Y_e smaller than the equilibrium electron fraction $Y_{e,eq}$. This results in a low electron Fermi energy, and consequently, relatively underluminous ν_e emission. For example: for the $\alpha = 0.03$ disk, material within the disk at $r = 10^{6.2}\text{ cm}$ has $Y_e/Y_{e,eq} \approx 0.7$ and neutrinos originating from this region are characterized by $R = 1.2$. By themselves, neutrinos from a region like this would tend to drive the outflow *neutron* rich. However, relativistic effects quash the influence of neutrinos from the innermost regions of the disk. The neutrino capture rate far above the disk goes approximately as the fifth power of the redshift factor $h = \sqrt{1 - 2M/r_0}$ (e.g. Puet, Fuller, & Cardall (2001)). This reduces the influence of neutrinos from $r_0 = 10^{6.2}\text{cm}$ by about an order of magnitude relative to the influence of neutrinos from $r = 10^{6.5}\text{cm}$. For disks accreting more rapidly than $\approx 1M_\odot \text{sec}^{-1}$, the inner regions become opaque to neutrinos and a more careful treatment of the neutrino spectrum is needed (Surman & McLaughlin 2003).

The above considerations about Y_e are exemplified in Table 1. In all cases the asymptotic electron fraction is larger than the in-disk electron fraction. The scaling of final Y_e with r_0 , ξ , and α has clear origins. All else being equal, a smaller α implies a denser disk, with faster weak interaction rates. In addition, a higher density implies - for a given mass loss rate - a lower outflow velocity and more time for weak processes to operate. These are the reasons why Y_e is so large in the $\alpha = 0.03$ disk. Similar reasons are behind the scaling of Y_e with r_0 . A smaller r_0 implies a larger density. As well, the entropy of the outflow (and the relative importance of positron capture) increases with decreasing r_0 . Lastly, as ξ_z increases, the

wind material is flung out centrifugally, attaining larger velocities at smaller distances from the disk, and there is less time for positron capture. This is why the asymptotic electron fraction in the $\xi_z = 4r_0$ case is relatively low.

Though disks with low α (or high \dot{M}) can be very neutron rich (Pruet, Woosley, & Hoffman (2003); Beloborodov (2003)), wind-like outflows will not preserve the neutron excess. In particular, wind-like outflows as discussed here cannot result in an asymptotic $Y_e \lesssim 0.4$. An exception to this is for the relativistic jet originating very near the black hole. Neutrino-antineutrino annihilation and relativistic effects dominate such ultra-relativistic outflows and they can remain neutron rich (Pruet, Fuller, & Cardall 2001).

It should be noted that we may overestimate the electron-fraction in the $\alpha = 0.1$ disk. This is because our calculation shows about half of the change in Y_e coming within one-pressure scale height of the disk mid-plane. Though our calculations show the outflow to be in near hydrostatic equilibrium near the disk, a two-dimensional calculation of the disk structure and composition would give a clearer picture of how Y_e evolves in outflows from the disk. The uncertainty in Y_e is unfortunate because efficient ^{56}Ni synthesis hinges sensitively on Y_e being larger than 0.5. For the $\alpha = 0.03$ disk, the asymptotic Y_e is less sensitive to the vertical disk structure (at least in our simple calculations) because most of the change in Y_e occurs a few pressure scale-heights above the disk mid-plane.

3.2.3. The Dynamical Timescale

Both the final entropy and electron fraction are set by processes near the disk. By contrast, the dynamic timescale at the epoch of nucleosynthesis is determined by the wind structure at $r \sim 2 - 5 \times 10^8 \text{ cm}$. One way to estimate the timescale characterizing the expansion of the fluid at $T \lesssim 1/2 \text{ MeV}$ is simply to use the calculated wind profiles. This is likely not correct. It seems implausible to expect that the disk outflow will remain well collimated in quasi-cylindrical geometry for $z \gtrsim 10r_0$. More likely is that the magnetic or pressure confinement breaks down at large radii and the wind assumes a quasi-spherical expansion and begins to coast. A further dynamical effect may also influence τ_{dyn} at large radius: when outflow encounters the overlaying stellar mantle, which also happens in NS winds, the wind will be slowed.

For lack of a calculation of the interaction between the disk wind and the exploding star, we make the assumption that after the sonic point the wind begins expansion with $a \propto r^2$ (here a is the area defined in eq. 8). While the wind has appreciable enthalpy the expansion is roughly homologous with $v \propto r$ and a dynamic timescale $\tau_{\text{dyn}} = r/v$. Entropy

and mass conservation imply the scaling $T \propto \rho^{1/3} \propto 1/r$. Once the velocity asymptotes to v_f a coasting phase described by $\rho v_f r^2 = \text{const.}$ follows. In the coasting phase the dynamic timescale is again approximately r/v_f , though it is now an increasing function of radius. In Table 2 we list the dynamic timescales calculated as described here. The first τ_{dynamic} listed for each calculation is that appropriate for homologous expansion ($r_{\text{sonic}}/v_{\text{sonic}}$). The second dynamic timescale listed is that for the flow when it is coasting. For consistency with the first definition of τ_{dyn} this dynamic timescale is defined as the time needed for the temperature to decrease by a factor of e from $T_9 \equiv T/10^9 K = 5$. The two different dynamic timescales should approximately bracket the plausible range of dynamic timescales.

Determining the dynamic timescale is equivalent to determining the mass outflow rate

$$\dot{M}^{(\text{sph})} \equiv 4\pi r^2 \rho v_f \quad (23)$$

for a given asymptotic entropy. Here $\dot{M}^{(\text{sph})}$ is the mass outflow rate that would obtain if the outflow were spherical. For winds from the inner regions of accretion disks the true mass outflow rate is typically much smaller than $\dot{M}^{(\text{sph})}$ because of the collimation of the wind. Observations of ^{56}Ni from GRBs may help constrain $\dot{M}^{(\text{sph})}$ (see below). Taking $r \approx v_f t$ gives the time at which a given temperature is reached in the outflow

$$t = 0.022 \text{ sec} \sqrt{\frac{\dot{M}_{-1} s_{30}}{v_{0.1}^3}} \left(\frac{0.5 \text{ MeV}}{T} \right)^{3/2}. \quad (24)$$

Here $\dot{M}_{-1} = \dot{M}^{(\text{sph})}/0.1 M_{\odot} \text{ sec}^{-1}$, $s_{30} = s_{\text{rad}}/30$, and $v_{0.1} = v/0.1c$. Equation (24) determines the coasting dynamic timescale (i.e. the temperature e-folding time when $T_9 = 5$) as $\tau_{\text{dyn}} = 0.1 \text{ sec} \sqrt{\dot{M}_{-1} s_{30} / v_{0.1}^3}$.

At some point the wind from the disk will encounter the overlaying stellar mantle. This will influence nucleosynthesis in the wind if the wind is slowed before $r \approx 2 \times 10^8 \text{ cm} \sqrt{\dot{M}_{-1} s_{30} / v_{0.1}}$, where $T_9 \approx 2.5$. At times less than a few seconds after disk/black hole formation, then, a simple wind picture is inadequate. For winds leaving the disk at times greater than a few seconds after disk formation the wind/envelope interaction is not important if the wind is energetic. Calculations by MacFadyen & Woosley (1999) show that at $t = 9.48 \text{ sec}$ the wind has cleared a region out to $r \gtrsim 3 \cdot 10^9 \text{ cm}$ in the star. Calculations by Maeda & Nomoto (2003) of outgoing bi-polar jets - whose influence on the star may roughly approximate the influence of the disk wind - show that by $t = 5 \text{ sec}$ outflow along the rotation axis continues uninhibited out to $r \sim 2.5 \cdot 10^{10} \text{ cm}$. This is somewhat faster than the shock velocities typical of ordinary core collapse SNe ($v_{\text{shock}} \sim 10^9 \text{ cm s}^{-1}$).

Though the wind/envelope interaction is not expected to influence nucleosynthesis in the wind, interaction of the wind with the stellar mantle will ultimately slow the outflow

and influence the observed Ni velocity. As a very rough estimate, if $2M_{\odot}$ of Ni-rich ejecta mixes with $10M_{\odot}$ of stellar mantle, the observed Ni velocity will be a factor of $\sqrt{2/10} \sim 1/2$ smaller than the estimates in Table 1.

3.2.4. *The influence of nuclear recombination on the wind dynamics*

During α recombination the total entropy is constant (apart from the influence of external heating sources), but entropy is transferred from the nucleons to the e^{\pm}/γ plasma. The amount of entropy transferred can be seen from eq. (12). For the modest entropy outflows discussed here, $\ln(T_{\text{MeV}}^{3/2}/\rho_8) \approx 3$ during recombination. So, the pair plasma gains about $(12 + 3) - (1/4)(15.4 + 3) \approx 10$ units of entropy. An equivalent way to estimate the entropy transfer is to note that α -particles are bound by $\sim 7.074\text{MeV/nucleon}$, so $\Delta s \approx 7.07\text{MeV}/T_{\text{rec}} \approx 10$, where $T_{\text{rec}} \approx 0.7\text{MeV}$ is the recombination temperature. ^{56}Ni is bound by 8.6 MeV/nucleon. This means that synthesis beyond He will add more energy to the pair plasma. Our calculations neglect the influence of this extra energy input on the wind dynamics. In part, this is because of the difficulty of coupling a nuclear network to our calculations, and in part because the lion’s share of the energy release is from α -recombination (7 out of 8.6 MeV).

Roughly speaking, nuclear recombination can influence the wind dynamics in two different ways. If recombination occurs below the sonic point there is the potential for the shift in entropy (as well as pressure and energy) from nucleons to the pair plasma to change the amount of viscous and neutrino heating suffered by the outgoing wind. This would change the asymptotic entropy, the mass outflow rate, and the electron fraction in the wind. Of the models we discuss in this paper, only the $\alpha = 0.03$ disks have outflows with sonic point temperatures below the recombination temperature. For these we have calculated wind solutions with and without alpha recombination. The winds without alpha recombination are equivalent to assuming that alpha particles are unbound. As can be seen from Tables 1 and 4, alpha recombination has a modest influence on our estimates of the asymptotic entropy and mass outflow rate. This is not so surprising, since recombination occurs at relatively low temperatures and after most of the heating has occurred.

The second, and most important effect of recombination is simply to make the nuclear binding energy available for kinetic energy (eq. 17). Indeed, as Woosley & Heger (2003) have pointed out, the observed kinetic energy for SN2003dh ($\sim 2.6 - 4 \cdot 10^{52}\text{erg}$) is not so different from the energy liberated by recombination of a solar mass of free nucleons to Ni ($\sim 1.65 \cdot 10^{52}\text{erg}$). Observationally, though, it still cannot be determined if Ni recombination accounts for essentially all of the observed kinetic energy, or only $\sim 1/3$ of the observed

kinetic energy. Our simple calculations indicate that Ni recombination accounts for about 70% of the kinetic energy of SN2003dh if the accretion disk has $\alpha = 0.03$, and about 25% of the kinetic energy if the accretion disk has $\alpha = 0.1$.

3.3. Outflows Flung Magnetically from the Disk

In the above discussion we assumed that the bulk of the work in driving the outflow is done by pressure/entropy gradients established by viscous and neutrino heating. It is also possible that material can be flung outward along a magnetic field line with little or no help from pressure gradients. This case has been thoroughly discussed by Blandford & Payne (1982), who showed that such outflows might mediate angular momentum transfer in tenuous accretion disks. In collapsar environments it is unclear to what extent such a mechanism can operate because the outflows are so dense and their inertia is important.

It is worth noting, though, that outflows centrifugally pushed along a magnetic field line can be qualitatively different from the wind-like outflows discussed above. In general they are neutron-rich and do not synthesize ^{56}Ni . The asymptotic entropy and electron fraction can both be very low - even lower than the in-disk values if neutrino cooling is important. For example, if θ_0 for model D is changed to 70° , then the asymptotic entropy and Y_e become ≈ 23 and ≈ 0.46 respectively. This can be understood from the discussion of the Bernoulli integral in section 3.2.1. For $\theta_0 = 70^\circ$ and $\xi_z = 2r_0$, the rotational velocity at $z = 2r_0$ is about 50% larger than the keplerian velocity there, so that thermal heating does not have to do much work (i.e. $1 + U_c$ is small). If $\theta_0 = 70^\circ$ and $\xi_z = 1r_0$, so that heating must do the work against gravity, the asymptotic entropy and electron fraction are essentially the same as for $\theta_0 = 80^\circ$ ($s = 28, Y_e = 0.50$). To summarize, the larger that magnetic or other effects keep $r\dot{\phi}$, the smaller will be the final entropy and electron fraction.

3.4. Nucleosynthesis in Winds

Here we concentrate on the synthesis of radioactive ^{56}Ni . There is no significant production of r -process elements for the high electron fractions and modest entropies found in our calculations. Although material leaving the disk from very near the hole will have higher entropy, Y_e will be too large for the r -process except perhaps in outflows with very rapid expansions (Meyer 2002).

Winds that are accelerating at the epoch of nucleosynthesis ($T \sim 0.5$ MeV) generally expand too quickly for efficient Ni production. There is no time for the 3-body reactions

that lead to ^{12}C synthesis and efficient α -captures. In contrast, the evolution and nucleosynthetic yields of winds that are not accelerating, but coasting, are largely described by two parameters (see eq. 24). For convenience we take these to be the asymptotic entropy s and

$$\beta \equiv \frac{\dot{M}_{-1}}{v_{0.1}^3} \propto \tau_{\text{dyn}}^2. \quad (25)$$

Ni synthesis also depends on Y_e , though the final Ni mass fractions do not vary greatly for $0.5 \lesssim Y_e \lesssim 0.53$.

In Figure 3 we show final Ni mass fractions as a function of the entropy and the parameter β . Large Ni mass fractions are favored by lower entropies and larger β 's. At an entropy of 50, which is obtained in material leaving the disk from $r_0 \lesssim 3 \times 10^6 \text{ cm}$, Ni synthesis is inefficient unless $\dot{M}_{-1}/v_{0.1}^3 \gtrsim 4$. For material with an entropy of 30, which is characteristic of material leaving the disk at $r \sim 10^7 \text{ cm}$, Ni synthesis is efficient ($X_{\text{Ni}} > 0.25$) as long as $\dot{M}_{-1}/v_{0.1}^3 > 1/4$. We note again that the \dot{M} here is the isotropic equivalent mass outflow rate. The true outflow rate is smaller because the Ni-wind is confined to a fraction of the solid angle above the disk.

As far as Ni synthesis in collapsars is concerned, our results are promising. Table 4 lists the mass outflow rates and final Ni mass fractions for the different wind calculations. Note that the mass outflow rates in Table 4 are representative of the “true” mass outflow rates, and that $\dot{M}^{(\text{sph})}$ (defined through eq. 23) is much larger. The outflows we calculate for material leaving the disk at 10^7 cm all efficiently synthesize Ni and have rather fast expansion velocities $v \gtrsim 0.1c$. However, the simple considerations presented here suggest that a low-alpha disk may have trouble synthesizing $\sim 0.5M_{\odot}$ of Ni. The reason is that such a disk is efficiently cooled by neutrino losses, so that the disk material is tightly gravitationally bound (see the Bernoulli parameters in Table 3), and heating cannot drive large mass outflow rates. For the $\alpha = 0.03$ disk, the mass outflow rates are about an order of magnitude smaller than for the $\alpha = 0.1$ disk. For the $\alpha = 0.1$ disk our models predict outflow rates $4\pi r_0^2 \rho_0 v_0 \sim 0.07M_{\odot} \text{ sec}^{-1}$ for $r_0 = 10^7$ and a factor of about 3 smaller for material leaving the disk from $r_0 = 10^{6.5} \text{ cm}$. These numbers are in the right range for explaining a total disk ejecta mass of $\sim 2M_{\odot}$ from an event with a duration typical of long duration GRBs ($\sim 10 - 100 \text{ sec}$).

4. Impulsive Rapid Mass Ejection: Magnetic Bubbles

We imagine a background disk wind, similar to the solutions obtained in the preceding section, but modulated by rapid impulsive events due to magnetic reconnection. Highly magnetic (low $\eta = P/(B^2/8\pi)$) filaments may be formed in the disk mid-plane and emerge

into the steady wind background rapidly as they expand and accelerate in the approximately exponential atmosphere of the disk. We propose here that this environment will have modest entropy, but low electron fraction (similar to the Y_e that obtains at the disk mid-plane) on account of the rapid expansion of the bubbles. It is in these events that $A \sim 130$ r -process elements may be synthesized.

There is an important difference between heating from magnetic instabilities and heating in an alpha-disk model. The viscous heating rate in an alpha-disk tracks the density. In eq. (11), for example, it is seen that $\dot{s} \sim P/(\rho T) \sim \text{Constant}$, so that very rapid increases in entropy can not be obtained in such a model. By contrast, heating from magnetic instabilities depends on the geometry of the magnetic fields. There is nothing to prevent heating in a relatively baryon dilute region (say two pressure scale heights above the disk mid-plane). Such heating can result in rapid, large increases in the entropy of the outflowing material. This basic idea is behind a number of suggestions for the origin of relativistic outflow in GRBs (Narayan, Paczyński, & Piran 1992; Kluzniak & Ruderman 1998).

To see how bubbles might form in the collapsar accretion disk, consider the following argument adapted from Kluzniak & Ruderman (1998), who studied differentially rotating neutron stars. For simplicity, consider an isothermal disk with a structure and equation of state given by

$$\rho(z) = \rho_0 \exp(-z) \quad (26)$$

$$s(z) = T^{3/2}/\rho = s_0 \exp(z) \quad (27)$$

$$P(z) = \rho T = P_0 \exp(-z). \quad (28)$$

Here we have assumed the gas to be dominated by free nucleons in the disk and have scaled the height above the disk in units of the disk scale height H . A fluid element rising adiabatically from the mid-plane of the disk will be in pressure equilibrium with the background fluid. If there is no magnetic pressure, then this element (denoted with the subscript b) will have a density

$$\rho_b = \rho_0 \exp(-3z/5) > \rho(z), \quad (29)$$

which implies that the fluid element will fall back to the mid-plane. If the fluid element carries a magnetic pressure P_M , pressure equilibrium with the background disk implies

$$\rho_b = \rho_0 \exp(-3z/5) \left(1 - \frac{P_M}{P(z)}\right)^{3/5}. \quad (30)$$

If the magnetic pressure is large enough then $\rho_b < \rho(z)$ and the fluid element will be buoyant. The force per unit volume on the fluid element is $\Omega_k^2 z$, which gives the equation of motion

$$\ddot{z} = z \left(\frac{\rho(z)}{\rho_b} - 1 \right). \quad (31)$$

Here we have scaled time in units of Ω_k^{-1} . If we make the simple assumption that the magnetic pressure increases linearly with time and $P_M = \eta P_0(t/2\pi)$, then eq. (31) becomes

$$\ddot{z} = z \left[\exp(-3z/5) \left(1 - \frac{\eta t}{2\pi} \exp(z) \right)^{-3/5} - 1 \right]. \quad (32)$$

This equation can be solved for $z(t)$ to provide an estimate of $P_M(z)$ and the entropy increase of the bubble as a function of the reconnection height. As a simple approach, suppose that an element rises one pressure scale height per radian that the disk rotates, or $z = t$ in our notation. This is a reasonable assumption since the magnetic pressure quickly becomes large compared to the disk pressure as the filament rises. If $z \approx t$, the ratio of magnetic energy density to thermal energy density evolves approximately as

$$\frac{P_M}{\rho_b T_b} = \frac{\eta z}{2\pi \exp(-z) - \eta z}. \quad (33)$$

If the energy in magnetic fields is transferred to thermal energy of the buoyant bubble the fractional increase in entropy of the bubble is approximately the ratio given in eq. (33). As an example, suppose that the initial magnetic field is 10% of the equipartition field ($\eta = 0.1$). If the energy in magnetic fields is transferred to the bubble at 1 disk-scale height above the mid-plane the fractional increase in entropy will be $\approx 6\%$. If the energy is transferred at three scale heights above the mid-plane, entropy will increase by a factor of ~ 23 .

To assess if the above argument seems plausible, let us assume that the magneto-rotational instability (the MRI; Balbus & Hawley 1994; Balbus & Hawley 1998) operates in collapsar disks and that this produces the turbulent viscosity necessary for accretion. Then, the local saturation magnetic field at a radius r_0 will be in rough equipartition with the azimuthal kinetic energy density;

$$\frac{B_{\text{sat}}^2(r_0)}{8\pi} \sim \frac{1}{2} \rho v_\phi^2 \quad (34)$$

where $v_\phi = r_0 \Omega_k = r_0 (GM/r_0^3)^{1/2}$. Empirically, for simulations of the MRI in accretion disks (Hawley, Gammie, & Balbus 1996) the magnetic field saturates at a sub-equipartition value, typically $1/2\pi$ times the field estimated from eq. (34). Taking this into account,

$$B_{\text{sat}}(r_0) \sim 1 \times 10^{14} \text{ G} \rho_9^{1/2} M_3^{1/2} r_{07}^{-1/2}, \quad (35)$$

where $\rho_9 = \rho/10^9 \text{ g cm}^{-3}$, $r_{07} = r_0/10^7 \text{ cm}$ and $M_3 = M/3M_\odot$. This magnetic field strength is in the right range for explaining modest entropy increases in the disk material. If the MRI is operating, the time to build a magnetic field is set by Ω_k^{-1} . The timescale for the maximum growing mode is

$$\tau_{\text{Max}} = 4\pi \left| \frac{d\Omega_k}{d \ln r} \right|^{-1}. \quad (36)$$

Roughly, we may assume that the local magnetic field may be entirely built and dissipated in τ_{Max} . Using eq. (34), and estimating the reconnection time as $\tau_{\text{Rec}} \approx \tau_{\text{Max}} = L_{\text{Rec}}/v_A$, where v_A is the Alfvén speed, we find that the characteristic length scale for reconnections $L_{\text{Rec}} \sim 115$ km. This may seem uncomfortably large, but we note that the τ_{Rec} above is the minimum required – we should perhaps require 3-4 doublings of the field at r_0 before dissipating. In this case, the reconnection time would be longer and L_{Rec} would be commensurately smaller. We expect these reconnection events to happen impulsively, and be separated in time by $\sim \tau_{\text{Rec}}$.

A bubble will begin to rise after entropy is deposited in a localized region. If the bubble is formed in a region of the disk where approximate hydrostatic equilibrium obtains, the bubble height z will evolve as

$$z \approx z_0 \Omega_k t. \quad (37)$$

Here we have made use of the fact that the gravitational force in the vertical direction is approximately $\Omega_k^2 z$. The characteristic length scale z_0 is taken here to be the pressure scale height H in the disk. The rising bubble will be in pressure equilibrium with the background fluid. This implies that initially the temperature evolves according to

$$T \propto \exp(-z/4H) \quad (38)$$

provided that the bubble is radiation dominated. These considerations suggest that the timescale characterizing the initial expansion of the bubble should be of order $\tau_{\text{initial}} \approx 10/\Omega_k \approx 0.01$ sec. Noting that the positron capture rate is $\lambda_{e+n} \approx 11 \text{ sec}^{-1} (T/3 \text{ MeV})^5$ gives an estimate of the change in Y_e of the outgoing bubble

$$\Delta Y_e \approx 0.2 \left(\frac{T_0}{3 \text{ MeV}} \right)^5 \left(\frac{\tau_{\text{initial}}}{0.01 \text{ sec}} \right). \quad (39)$$

Here T_0 is the temperature of the bubble formed after magnetic reconnection. We note that for the $\alpha = 0.03, \dot{M} = 0.1 M_\odot \text{ sec}^{-1}$ disk, the height averaged disk temperature is $\sim 2.2 - 2.8 \text{ MeV}$ for $r_0 < 10^7 \text{ cm}$. Bubbles can retain low values of Y_e .

Equations (37) and (38) are appropriate for characterizing the bubble passage through the region of the disk that is in approximate hydrostatic equilibrium. Those equations are not appropriate for estimating the expansion timescale at the late times and low temperatures important for nucleosynthesis. The expansion timescale at $T \sim 0.5 \text{ MeV}$ depends on the profile of the background wind. If the background wind is radiation dominated well above the disk, then pressure equilibrium between the bubble and wind implies that the temperatures in the wind and bubble are equal. In this case the expansion timescale of the wind (τ in Table 2) may be used as a rough indication of the expansion timescale of the bubble.

4.1. Nucleosynthesis in Bubbles

As discussed in the introduction, there are indications that the site of the $A \lesssim 130$ r -process nuclei is different from the site of the r -process nuclei with $A \gtrsim 130$. In particular, observations of ultra-metal poor stars (e.g. Sneden et al. 1996; Burris et al. 2000) and inferences from elemental abundances in pre-solar meteorites (Wasserburg, Busso, & Gallino 1996) suggest that the $^{135,137}\text{Ba}$ isotopes are not significantly produced in the same events that produce $^{127,129}\text{I}$ and lighter r -process elements. An exhaustive survey of how a nuclear burning site can produce a near solar abundance pattern of nuclei near one of the r -process peaks, while leaving the other peaks unpopulated, is beyond the scope of this paper. Here we show in broad stroke that conditions in collapsars are favorable for the synthesis of the $A \sim 130$ r -process elements. In the spirit of investigation, we also discuss a way in which a near-solar abundance pattern of (only) $A \leq 130$ r -process elements can be synthesized.

Neutron-rich outflows characterized by rapid expansion generically synthesize r -process elements (e.g. Hoffman, Woosley, & Qian (1997)). As an example, we show in Fig. 4 results of nucleosynthesis calculations for outflows with $Y_e = 0.2$, a temperature e-folding time $\tau = 0.12$ sec, and three different entropies. These conditions are close to those we estimate may obtain in outflows from the inner regions of accretion disks with $\alpha = 0.03$ and $\dot{M} = 0.1M_\odot \text{ sec}^{-1}$. Here the (unnormalized) overproduction factor for nucleus j is defined as

$$O(j) = \frac{X_j}{X_{\odot,j}}, \quad (40)$$

where X_j is the mass fraction of the nucleus j in the bubble and $X_{\odot,j}$ is the mass fraction of the nucleus in the sun. Though it is evident from Fig. 4 that some r -process elements are synthesized, good agreement with the solar abundance pattern is not obtained.

It is unreasonable to expect that a single type of bubble will prevail in the dynamic collapsar environment. Rather, a broad spectrum of bubbles, with different entropies, dynamic timescales, electron fractions, and so on will be created. To investigate the average nucleosynthesis we generated random bubbles with properties defined according to

$$s = 50 + 50r \quad (41)$$

$$Y_e = 0.15 + 0.25r \quad (42)$$

$$\tau = 0.03(1 + 4r) \text{ sec} \quad (43)$$

$$T_{9,\text{mix}} = 1 + 2r. \quad (44)$$

Here r is a random number between 0 and 1 and is generated separately for each of eqs. (41-44). The choices for Y_e and τ above were adopted because they represent the expected range of conditions in high entropy outflows from the inner regions ($r \lesssim 10^7 \text{ cm}$) of a disk with

$\alpha = 0.03$ and $\dot{M} = 0.1M_{\odot} \text{ sec}^{-1}$. Choices for s and $T_{9,\text{mix}}$ are not well constrained. The parameter $T_{9,\text{mix}}$ is the temperature at which the bubble is assumed to mix with the proton-rich ambient medium. When the bubble shears or destabilizes, the free neutrons available for capture are diluted. To represent this we made the rough approximation that all neutron captures then cease and the abundance pattern of neutron rich elements is frozen in (except for β decays) for $T_9 < T_{9,\text{mix}}$. Because charged particle reactions are relatively slow for $T_9 \lesssim 3$ we expect this to be a fair approximation.

Average overproduction factors for one hundred bubbles generated as described above are shown in Fig. 5. Overall there is quite good agreement with the solar abundance pattern of $90 < A < 130$ r -process elements. Overproduction factors for ^{100}Mo , ^{107}Ag , ^{110}Pd , ^{116}Cd , ^{123}Sb and ^{124}Sn - elements principally or entirely synthesized in the r -process - are all within a factor of a few of the overproduction factor for ^{106}Pd . ^{127}I is underproduced by a factor of about 5. Most of the $A \sim 130$ nuclei have progenitors about 8 units from stability near the $N=82$ closed neutron shell in our calculations. Uncertainties in the location of the shell closures and the β decay rates of near-drip line nuclei may account for the modest underproduction of ^{127}I . ^{135}Ba and heavier elements are absent. In Fig. 6 we investigate the sensitivity of nucleosynthesis to the distribution of s and $T_{9,\text{min}}$ in the bubbles. Nucleosynthesis is relatively insensitive to modest changes in eqs. (41-44).

Our calculations indicate that typical overproduction factors for 2nd-peak nuclei are $\bar{O} \approx 5 \cdot 10^7$. With this, we can estimate how much mass collapsars have to eject as bubbles in order to account for the galactic inventory of $A < 130$ r -process nuclei. For events with the frequency of Type II SNe, studies of galactic chemical evolution indicate that a typical nuclide must have an overproduction factor

$$O(j) \approx 10 \frac{\bar{M}^{ej}}{M^b} \quad (45)$$

in order to account for the observed solar abundance of that nuclide (e.g. Mathews, Bazan, & Cowan (1992)). In eq. (45) $\bar{M}^{ej} \approx 10 - 20M_{\odot}$ is the typical mass ejected by a type II SN and $M^b X(j)$ is the mass of the nuclide j ejected. For collapsars, $O(j)$ must be $\sim 1/f_c$ larger, where f_c is the fraction of core collapse SNe that become collapsars. The total mass ejected as bubbles must then

$$M^b \approx 10^{-4} M_{\odot} \frac{0.1}{f_c} \frac{\bar{O}}{5 \cdot 10^7}. \quad (46)$$

If typical bubbles are formed with initial radius r_b , temperature T_b , and entropy s_b per baryon, eq. (46) implies that the number of bubbles needed per event is

$$n_b \approx 500 \frac{s_b}{50} \left(\frac{10^6 \text{ cm}}{r_b} \right)^3 \left(\frac{2 \text{ MeV}}{T_b} \right)^3 \frac{M_b}{10^{-4} M_{\odot}}. \quad (47)$$

Now, if the disk lasts for a time t , the number of disk revolutions, or magnetic field windings, per bubble is

$$n_{\text{wind}} = \frac{t\Omega_k}{2\pi n_b} \approx 8 \frac{t}{50 \text{ sec}} \frac{\Omega_k}{10^3 \text{ sec}^{-1}} \frac{10^3}{n_b}, \quad (48)$$

which is a reasonable number if magnetic instabilities take a few rotations to develop.

We have argued that if collapsars are only 1% as frequent as Type II SNe then each collapsar needs to eject $10^{-3}M_\odot$ of r-process bubbles in order to account for the total mass of 130-peak r-process material present in the galaxy today. This required ejecta mass is approximately 0.01% of the total mass ejected in a Ni wind and is roughly consistent with a description of bubbles as forming on a magnetic instability timescale and observed GRB durations. However, there still remains the more delicate issue of whether collapsars as the 130-peak site is consistent with observations of metal poor stars and what is known about galactic chemical evolution.

Unfortunately, much less is known about the production of the $A < 130$ elements than is known about the production of the heavier r-process elements. For example, while CS22892-052 and a handful of similar stars are thought to have been enriched by only one $A > 130$ production event, these authors are not aware of any stars thought to have been enriched by only a single $A < 130$ enriching event. Within the context of the models developed by Qian and Wasserburg this has an explanation in the relative rarity of the events which produce the second peak elements.

One type of argument which has been used to differentiate proposed *r*-process sites is based on an analysis of the refreshment rate of material in the interstellar medium (ISM). This argument has previously been used to assesss the viability of neutron star mergers as an *r*-process site and can also be applied to collapsars. Qian (2000) showed that enrichment of the ISM with second peak elements every 10^8 yr is consistent with the observed trend of Ag abundances with [Fe/H] in metal poor stars. Here we simply note that a refreshment frequency of $f_{\text{ref}} \approx (10^8 \text{ yr})^{-1}$ is consistent with enrichment of the ISM by collapsars. Following the notation of Qian (2000),

$$f_{\text{ref}} \approx (10^8 \text{ yr})^{-1} \left(\frac{f^{\text{SN}}}{(30 \text{ yr})^{-1}} \right) \left(\frac{f_c}{0.01} \right) \left(\frac{M_{\text{mix}}}{3 \cdot 10^5 M_\odot} \right), \quad (49)$$

where f^{SN} is the rate of type II SNe in the galaxy and M_{mix} is the total mass swept up by a collapsar remnant. Note that M_{mix} for collapsars is about an order of magnitude larger than the mass swept up by type II SNe. This is because the kinetic energy in the collapsar explosion is about ten times larger and because the swept up mass is proportional to $E_{\text{kinetic}}^{6/7}$ (Thornton et al. 1998).

5. Results and Conclusions

We have considered the nucleosynthesis which may attend outflows in the collapsar Gamma Ray Burst environment. Both wind-like outflows and bubble-like outflows were considered. Wind-like outflows may be relevant for recent observations of SN1998bw and SN2003dh, which hint at a robust connection between the central engines of GRBs and core-collapse SNe – or at least SN-like light curves. To power such light curves requires $\sim 0.5M_{\odot}$ of radioactive Ni moving outward very rapidly ($v \gtrsim 0.1c$ for SN2003dh). These are characteristics beyond the reach of canonical SNe with energies $\sim 10^{51}$ erg. The results of our simple models of viscosity and neutrino-driven winds are promising. Under a broad range of conditions such winds copiously produce fast moving radioactive Ni.

In general, winds from collapsar disks cannot preserve a large neutron excess. This implies that these winds will not synthesize interesting neutron rich elements. However, chaotic heating or buoyant magnetic filaments in localized regions in the disk result in bubbles which rise on a timescale comparable to a Kepler period. This is fast enough to preserve the neutron excess found in the mid-plane of the disk. Though we do not have a complete theory of bubble production, we have shown that the solar abundance pattern for $90 < A < 130$ r -process elements can naturally be produced in bubble-like outflows and that the requirements for the total mass ejected are plausible. As we have discussed, identification of collapsars as the source of the 2nd peak r -process elements is consistent with a number of observational indications.

We gratefully acknowledge Stan Woosley for guidance and many helpful suggestions. JP also acknowledges George Fuller for insightful comments. This research has been supported through a grant from the DOE Program for Scientific Discovery through Advanced Computing (SciDAC; DE-FC02-01ER41176). This work was performed under the auspices of the U.S. Department of Energy by University of California Lawrence Livermore Laboratory under contract W-7405-ENG-48. TAT gratefully acknowledges conversations with Eliot Quataert and is supported by NASA through Hubble Fellowship grant #HST-HF-01157.01-A awarded by the Space Telescope Science Institute, which is operated by the Association of Universities for Research in Astronomy, Inc., for NASA, under contract NAS 5-26555.

REFERENCES

Balbus, S. A. & Hawley, J. F. 1994, MNRAS, 266, 769
Balbus, S. A. & Hawley, J. F. 1998, Rev. Mod. Phys., 70, No. 1

Beloborodov, A. M. 2003, ApJ, 588, 931

Blandford, R. D. & Payne, D. G. 1982, MNRAS, 199, 883

Burbidge, E. M., Burbidge, G. R., Fowler, W. A., & Hoyle, F. 1957, Rev. Mod. Phys., 29, 547

Burris, D. L., Pilachowski, C. A., Armandroff, T. E., Sneden, C., Cowan, J. J., & Roe, H. 2000, ApJ, 544, 302

Cameron, A. G. W. 1957, PASP, 69, 201

Cardall, C. Y. & Fuller, G. M. 1997, ApJL, 486, 111

Daigne, K. & Mochkovitch, R. 2002, A&A, 388, 189

Duncan, R. C., Shapiro, S. L., & Wasserman, I. 1986, ApJ, 309, 141

Fuller, G. M., Fowler, W. A., & Newman, M. J. 1982, ApJ, 252, 715

Galama, T. J. 1998, Nature, 395, 670

Hawley, J. F., Gammie, C. F., & Balbus, S. A. 1996, ApJ, 464, 690

Heger, A., Fryer, C.L., Woosley, S.E., Langer, N. & Hartmann, D.H. 2003, ApJ, 591, 288

Hjorth, J. et al. 2003, Nature, 423, 847

Hoffman, R. D., Woosley, S. E., & Qian, Y.-Z. 1997, ApJ, 482, 951

Iwamoto, K. et al. 1998, Nature, 395, 672

Kluzniak, W. & Ruderman, M. 1998, ApJ, 505, L113

Macfadyen, A. I. 2003, astro-ph/0301425

MacFadyen, A. I. & Woosley, S. E. 1999, ApJ, 524, 262

Maeda, K. & Nomoto, K. 2003, ApJ, accepted

Mathews, G. J., Bazan, G., & Cowan, J. J. 1992, ApJ, 391, 719

Meyer, B. 2002, Phys. Rev. Lett., 89, 231101

Mihalas, D. & Mihalas, B., *Foundations of Radiation Hydrodynamics*, New York, Oxford University Press, 1984

Nagataki, S., Mizuta, A., Yamada, S., Takabe, H. & Sato, K. 2003, ApJ, accepted

Narayan, R., Paczyński, B., & Piran, T. 1992, ApJL, 395, L83

Otsuki, K., Tagoshi, H., Kajino, T., & Wanajo, S.-Y. 2000, ApJ, 533, 424

Patat, F. et al. 2001, ApJ, 555, 900

Popham, R., Woosley, S. E., & Fryer C. L 1999, ApJ, 518, 356

Price, P. A. et al. 2003, ApJ, 589, 838

Pruet, J., Fuller, G. M., & Cardall, C. Y. 2001, ApJ, 561, 937

Pruet, J., Woosley, S.E., & Hoffman, R.D. 2003, ApJ, 586, 1254

Qian, Y.-Z. 2001, ApJL, 525, 117

Qian, Y.-Z. & Woosley, S.E. 1996, ApJ, 471, 331

Qian, Y.-Z., Vogel, P., & Wasserburg, G. J. 1998, ApJ, 494, 285

Qian, Y.-Z. & Wasserburg, G. J. 2000, Phys. Reps., 333, 77

Shakura, N. I. & Sunyaev, R. A. 1973, A&A, 24, 337

Sneden, C., McWilliam, A., Preston, G. W., Cowan, J. J., Burris, D. L., & Armosky, B. J. 1996, ApJ, 467, 819

Stanek, K. Z. et al. 2003, ApJ, 591 L17

Stone, S. M., Pringle, J. E., & Begelman, M. C. 1999, MNRAS, 310, 1002

Sumiyoshi, K., Suzuki, H., Otsuki, K., Teresawa, M., & Yamada, S. 2000, PASJ, 52, 601

Surman, R. & McLaughlin, G. C., 2003, ApJ, accepted, astro-ph/0308004

Takahashi, K., Witti, J., & Janka, H.-T. 1994, A&A, 286, 857

Thompson, T. A. 2003, ApJL, 585, L33

Thompson, T. A., Burrows, A., & Meyer, B. S. 2001, ApJ, 562, 887

Thornton, K., Gaudlitz, M., Janka, H.-Th., & Steinmetz, M. 1998, ApJ, 500, 95

Wanajo, S., Kajino, T., Mathews, G. J., & Otsuki, K. 2001, ApJ, 554, 578

Wasserburg, G. J. & Qian, Y.-Z. 2000, ApJL, 529, 21

Wasserburg, G. J., Busso, M., Gallino, R. 1996, ApJL, 466, L109

Woosley, S. E. 1993, ApJ, 405, 273

Woosley, S. E. & Baron, E. 1992, ApJ, 391, 228

Woosley, S. E., Wilson, J. R., Mathews G. J., Hoffman, R. D., & Meyer, B. S. 1994, ApJ, 433, 209

Woosley, S. E., Eastman, R. G., & Schmidt, B. P. 1999, ApJ, 516, 788

Woosley, S. E. & Heger, A., submitted to ApJ, astro-ph/0309165

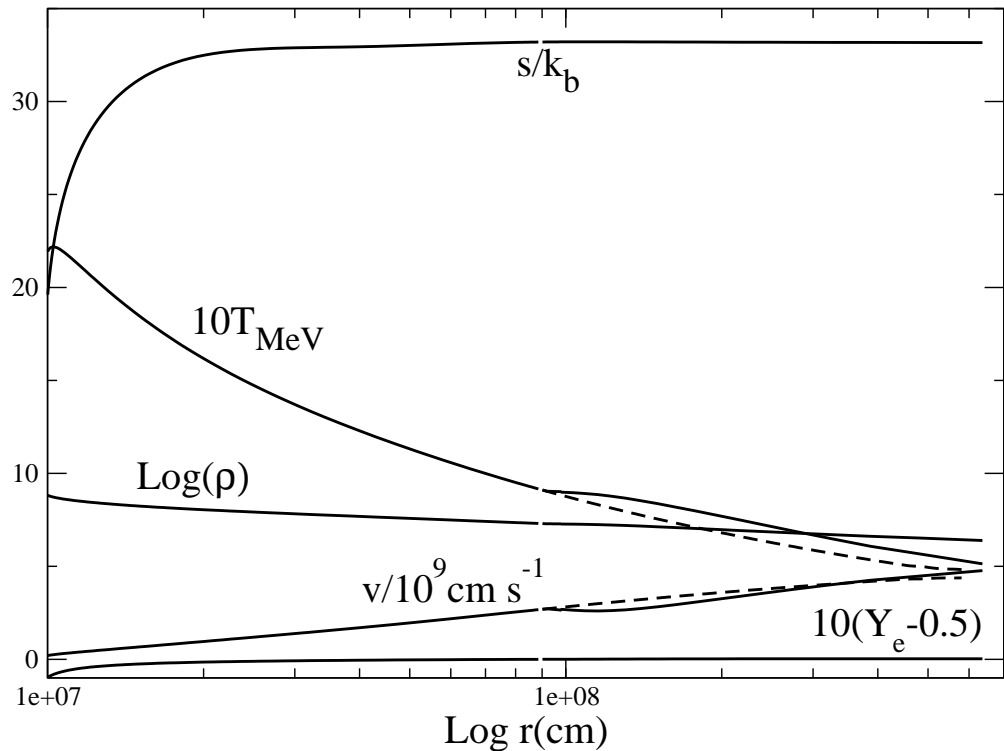


Fig. 1.— Wind for material beginning at $r_0 = 10^7$ cm from a disk with $\alpha = 0.1$ and $\dot{M} = 0.1 M_\odot \text{ sec}^{-1}$. The solid lines are for calculations including α -recombination, while the dashed lines are for calculations which neglect the influence of α recombination on the wind. Note that in our simple calculations most of the heating (entropy change) occurs near the base of the flow.

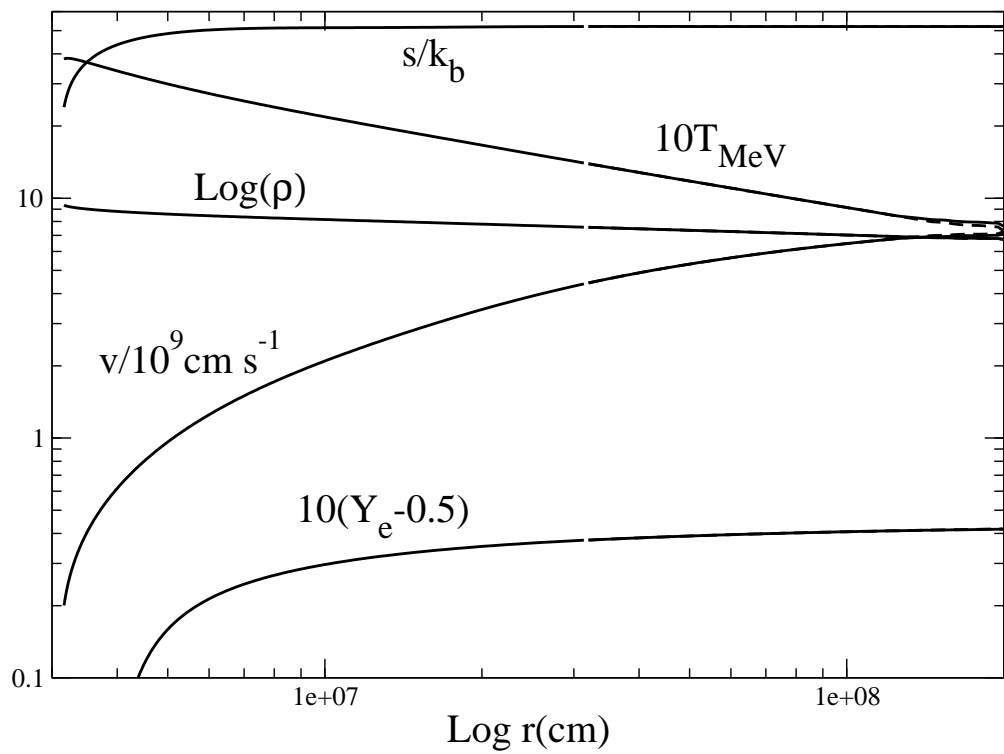


Fig. 2.— The same as Fig. 1 except for material beginning at $r_0 = 10^{6.5}$ cm. Note that this figure has logarithmic spacing on the vertical axis.

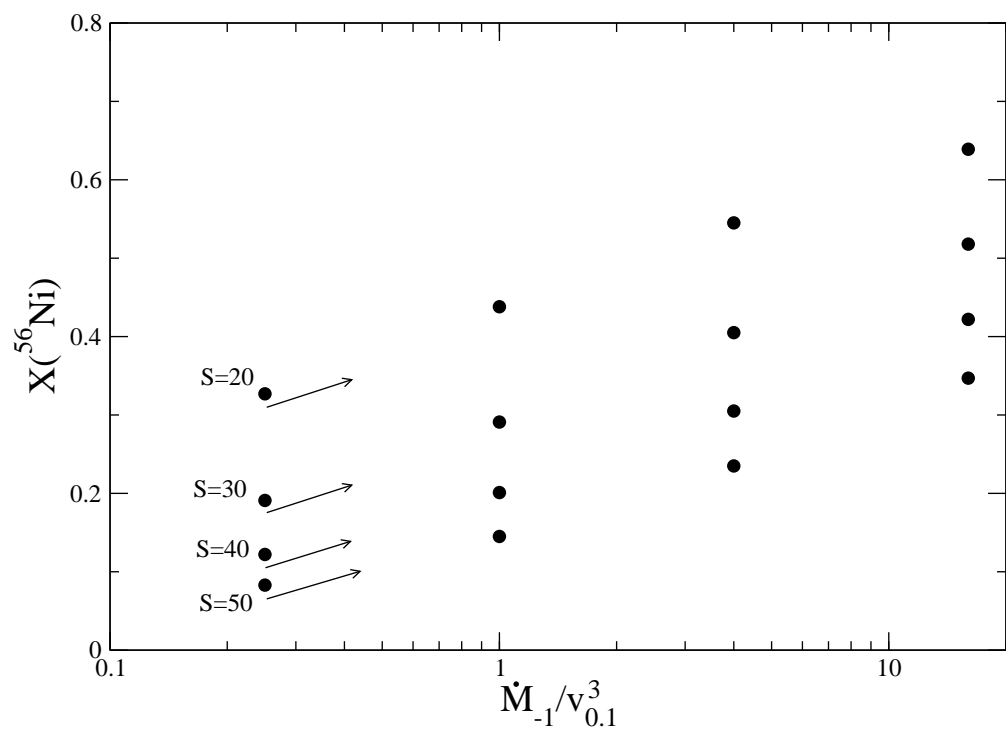


Fig. 3.— Plot of Ni mass fraction vs. the parameter β for different entropies. This plot assumes $Y_e = 0.51$.

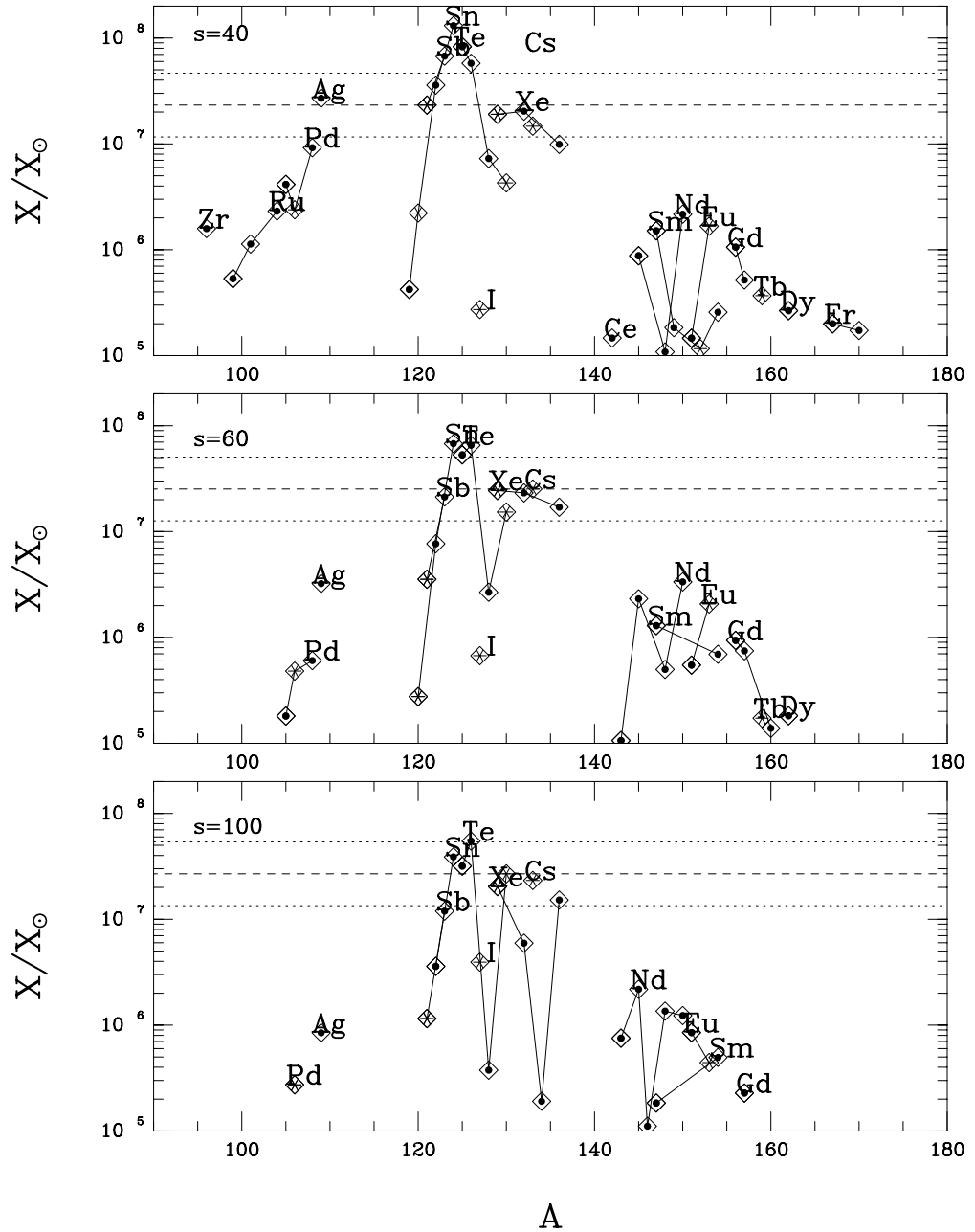


Fig. 4.— Overproduction factors for nuclei synthesized in bubbles with $Y_e = 0.2$, $\tau = 0.12$ sec, and different entropies. Solid lines connect isotopes of a given element. The most abundant isotope in the Sun for a given element is plotted as an asterisk. A diamond around a data point indicates the production of that isotope as a radioactive progenitor. Though some r -process elements are synthesized, agreement with the solar abundance pattern is poor.

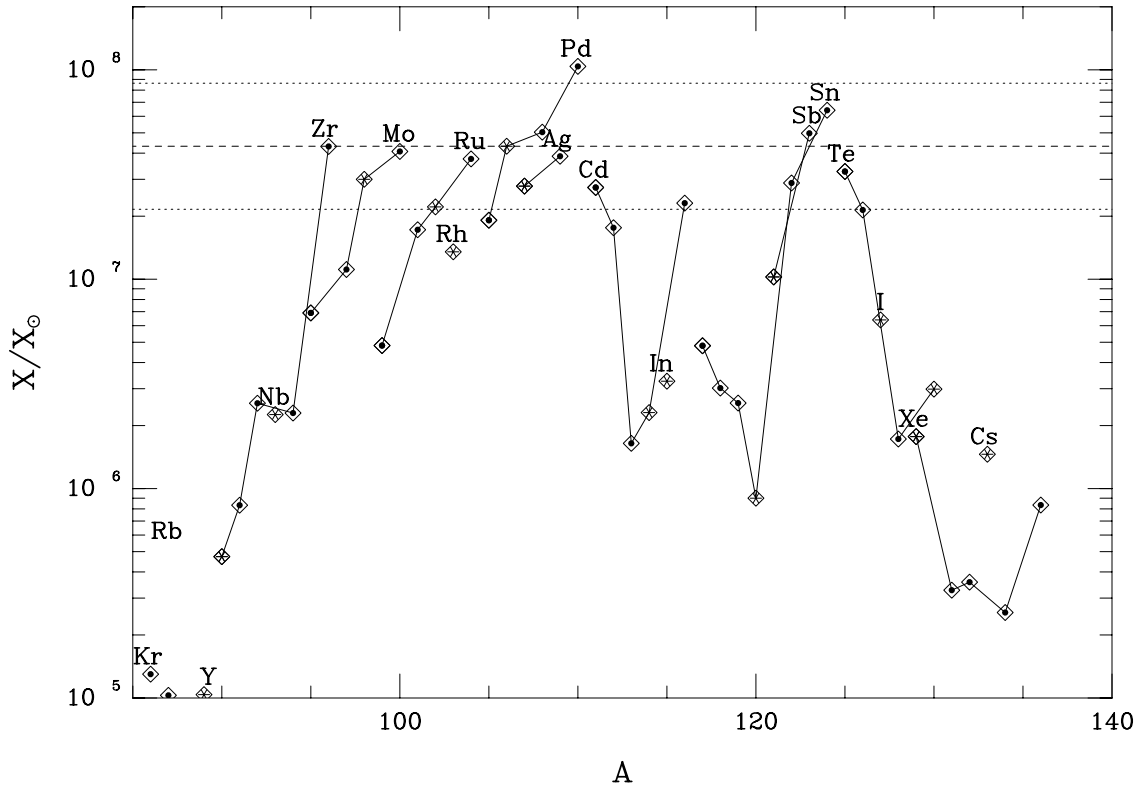


Fig. 5.— Average overproduction factors for 100 bubbles generated according to eqs. (41-44). Agreement with the solar abundance pattern of *r*-process elements with $A < 130$ is quite good, though ^{127}I is underproduced by a factor of about 4. Production of species heavier than $A = 130$ is negligible.

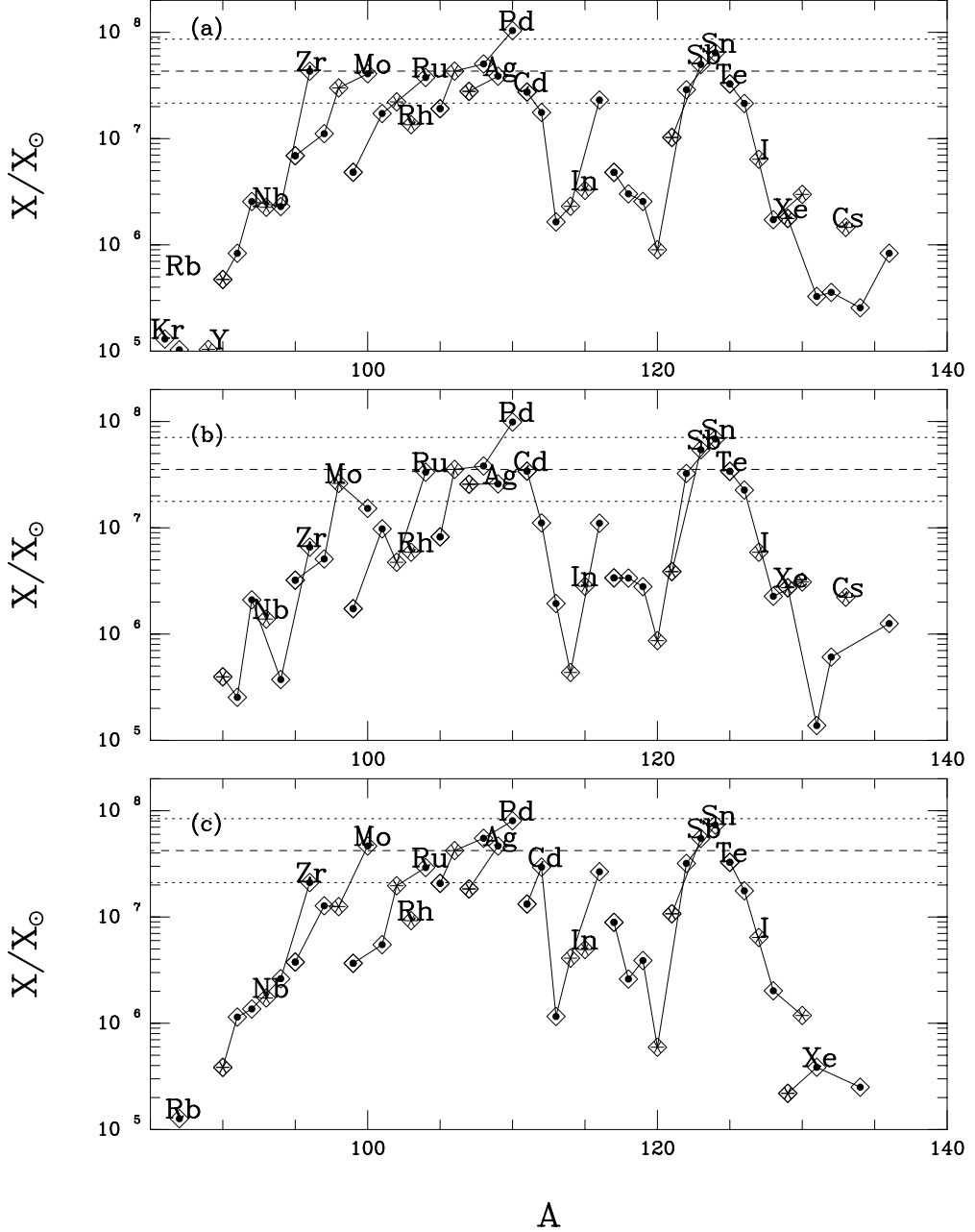


Fig. 6.— Influence of changing assumptions about the distribution of bubbles produced. Run (a) is the reference run and corresponds to the distribution of bubbles described by eq. (41-44). Run (b) is the same as run (a) except the entropy in the bubbles is assumed to be uniformly spread from $s = 50$ to $s = 150$. Run (c) is the same as run (a), except $T_{9,\min}$ is assumed to be uniformly spread from 1.5 to 3.5. In run (a) the average of 100 bubbles was taken while in runs (b) and (c) the average of 30 bubbles was taken.

Table 1. Wind characteristics for different parameters

Model	α	r_0 (cm)	ξ_z/r_0	$Y_{e,i}$	$Y_{e,f}$	s_f	v_f/c^2
A	0.03	$10^{6.5}$	2	0.12	0.56	54	0.21[0.17]
B	0.03	10^7	2	0.22	0.50 ¹	24 ¹	0.11[0.06]
C	0.1	$10^{6.5}$	2	0.44	0.54	52	0.36[0.34]
D	0.1	10^7	2	0.43	0.50	33	0.23[0.19]
E	0.1	$10^{6.5}$	4	0.44	0.50	47	0.32[0.30]
F	0.1	10^7	4	0.43	0.46	32	0.22[0.18]

¹For model B $s_f = 26$ and $Y_{e,f} = 0.53$ if alpha recombination is neglected. For all other models alpha recombination does not effect s_f or $Y_{e,f}$ in our calculations.

²Values in square brackets are those calculated if alpha recombination is neglected.

Table 2. Dynamic timescales for the different winds.

Model	$\tau_{\text{homologous}}$ (sec)	τ_{coast} (sec)
A	0.03	(NC) ^a
B	0.17	(NC) ^a
C	0.007	~ 0.04
D	0.03	~ 0.10
E	0.002	~ 0.03
F	0.012	~ 0.08

^aThe sonic-point temperature for these winds is less than 0.5MeV.

Table 3. Minimum values of the final entropy for a given final velocity

α	r_0 (cm)	b_i (MeV) ^a	$s_f(v_{\text{final}} = 0.1c)$	$s_f(v_{\text{final}} = 0.2c)$	$s_f(v_{\text{final}} = 0.3c)$
0.03	$10^{6.5}$	–132	53	58	66
0.03	10^7	–37	26	33	44
0.1	$10^{6.5}$	–83	45	49	56
0.1	10^7	–21	28	35	46

^aIn-disk value of the Bernoulli parameter (eq. 17).

Table 4. Mass ablation rate and estimated final ^{56}Ni mass fractions for some different wind calculations.

Model	$\dot{M}(M_{\odot} \text{ sec}^{-1})^{\text{a}}$	$X(^{56}\text{Ni})^{\text{b}}$
A	10^{-3}	$\lesssim 0.1$
B	4×10^{-3}	~ 0.5
C	3×10^{-2}	~ 0.1
D	7×10^{-2}	~ 0.4
E	6×10^{-2}	$\lesssim 0.1$
F	0.14	- ^c

^aDefined as $4\pi r_0^2 \rho_0 v_0$.

^bEstimated from Figure 3 under the assumption that the wind begins quasi-spherical expansion after the sonic point. Dynamic timescales were taken from Table 2.

^cThis model has $Y_e < 0.48$ and does not produce ^{56}Ni .